Journal of Alloys and Compounds 508 (2010) 292–296

Contents lists available at ScienceDirect

Journal of Alloys and Compounds

journal homepage: www.elsevier.com/locate/jallcom

Room temperature magnetic and magnetocaloric properties of $La_{0.67}Ba_{0.33}Mn_{0.98}Ti_{0.02}O_3$ perovskite

Ma. Oumezzine [a], S. Zemni [a,*], O. Peña [b]

[a] Laboratoire de Physico-chimie des Matériaux, Département de Physique, Faculté des Sciences de Monastir, Monastir 5019, Tunisia
[b] Sciences Chimiques de Rennes, UMR 6226-CNRS, Université de Rennes 1, 35042 Rennes, Cedex, France

ARTICLE INFO

Article history:
Received 3 June 2010
Received in revised form 23 August 2010
Accepted 24 August 2010
Available online 8 September 2010

Keywords:
Chemical synthesis
Microstructure
Magnetic materials
Magnetocaloric effect

ABSTRACT

The influence of Ti-doping on the magnetic and magnetocaloric properties of $La_{0.67}Ba_{0.33}Mn_{0.98}Ti_{0.02}O_3$ perovskite is investigated. $La_{0.67}Ba_{0.33}Mn_{0.98}Ti_{0.02}O_3$ sample was prepared by ceramic route at 1400 °C. It is a cubic Pm–3m single phase and exhibits a sharp ferromagnetic–paramagnetic (FM–PM) transition at a Curie temperature T_C (314 K) which is very close to room temperature. Above T_C the data follow a Curie–Weiss law with a shift between experimental and calculated effective paramagnetic moment. The associated experimental magnetic entropy change (ΔS_M) and the relative cooling power (*RCP*) have been determined. The observed field dependence of ΔS_M is explained reasonably well by the Landau theory of second order phase transition. The maximum entropy change $|\Delta S_M^{max}|$ exhibits a linear dependence with the applied magnetic field. $|\Delta S_M^{max}|$ and *RCP* are respectively 3.21 J kg^{-1} K^{-1} (21.48 mJ cm^{-3} K^{-1}) and 307 J kg^{-1} (2054 mJ cm^{-3}) at 5 T, which are about 30% of pure Gd. Our results on the magnetocaloric effect (MCE) are compared favourably with reported values for other doped manganites, thus concluding that our sample can be used as a magnetic refrigerant around room temperature.

1. Introduction

Magnetic refrigeration (MR) technology, based upon the magnetocaloric effect (MCE), is required near room temperature and is of particular interest considering the potential impact on energy savings and environmental protection. Gd is considered as a prototype material for such purpose, with a large MCE near its Curie temperature (293 K) [1,2]. But its usage is somehow commercially limited because the cost of Gd is quite expensive ~$4000/kg. Recently, an intense interest in perovskite-type manganese oxides (the so-called manganites) $R_{1-x}M_xMnO_3$ (where R is a rare earth ion and M is a divalent alkali) is prompted by the observation of colossal magnetoresistance (CMR) [3–5]. Because of some advantages over Gd and intermetallic alloys, such as low production cost, chemical stability, high resistivity (minimum Eddy current loss) [6] and not affected by corrosion, manganites have attracted more attention as alternative candidates for magnetic refrigeration in the vicinity of room temperature. $La_{0.67}Ba_{0.33}MnO_3$ perovskite compound has a relatively high Curie temperature ($T_C \approx 350$ K [7]). Potential applications, particularly the magnetic refrigeration (MR) require having transition temperatures T_C close to room temperature. This can be achieved by an appropriate amount of oxygen stoichiometry [8] or by substitution of Mn by a non-magnetic cation such as titanium. In this work we have investigated the magnetic and magnetocaloric properties of Ti-doped $La_{0.67}Ba_{0.33}Mn_{0.98}Ti_{0.02}O_3$ manganites. Theoretical modeling of the MCE is used in order to compare the experimental ($-\Delta S_M$) curve and the estimated one using Landau theory.

2. Experimental

Polycrystalline $La_{0.67}Ba_{0.33}Mn_{1-x}Ti_xO_3$ ($x = 0, 0.02$) samples were synthesized by solid-state reaction route at 1400 °C, using (Mn + Ti)/(La + Ba) ratio equal to 1 as reported elsewhere for $La_{0.67}Ba_{0.33}Mn_{1-x}Ti_xO_3$ ($0 \le x \le 0.3$) manganites [9]. Powder X-ray diffraction (XRD) analysis was carried out in Bragg–Brentano geometry with a "PANalytical X'Pert Pro" diffractometer with filtered (Ni filter) Cu radiation. Data for the Rietveld refinement were collected in the 2θ range of 10–100° with a step size of 0.017° and a counting time of 18 s per step. Scanning electron microscopy (SEM) was used to determine grain size and morphology of the sample. Energy dispersive X-ray fluorescence (EDX) analysis was used to determine chemical homogeneity and cations composition. Quantitative analyses of chemical elements, including the oxygen content, were performed by inductively coupled plasma atomic emission spectroscopy (ICPAES) techniques. Magnetization (M) vs. temperature (T) and magnetization vs. magnetic field ($\mu_0 H$) were measured using a MPMS-XL5 quantum design SQUID susceptometer. $M(T)$ data were obtained in 2–400 K temperature range with applied magnetic field of 0.01 T in field cooled (FC) and zero field cooled (ZFC) regimes. Isothermal $M(H)$ data were measured in 230–390 K temperature range by a step of 10 K under an applied magnetic field varying from 0 to 5 T.

* Corresponding author.
E-mail address: zemnis@yahoo.fr (S. Zemni).

0925-8388/$ – see front matter © 2010 Elsevier B.V. All rights reserved.
doi:10.1016/j.jallcom.2010.08.145

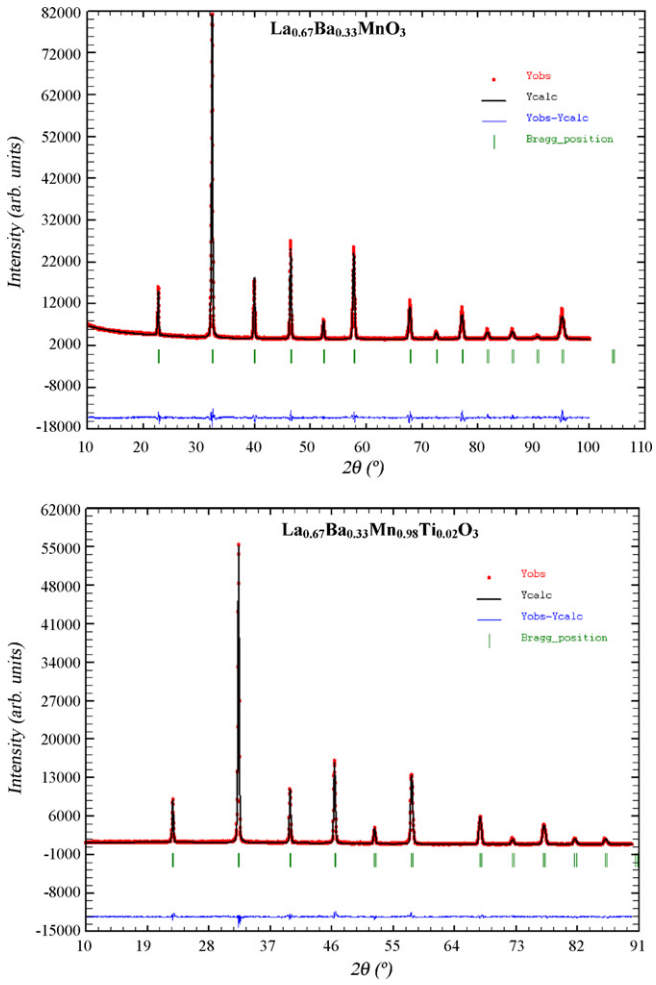

Fig. 1. Rietveld plot of XRD data for polycrystalline $La_{0.67}Ba_{0.33}Mn_{1-x}Ti_xO_3$ ($x = 0$, 0.02) compounds at room temperature. The points are the observed profile; the solid line is the calculated one. Tick marks below the profile indicate the position of allowed Bragg reflections. The line curve at the bottom gives the difference between observed and calculated profiles.

3. Results and discussions

3.1. Microstructure analysis

Fig. 1 presents the XRD patterns of $La_{0.67}Ba_{0.33}Mn_{1-x}Ti_xO_3$ ($x = 0$, 0.02) showing sharp peaks which could be indexed in the cubic symmetry. No impurity phases were detected within the XRD limits. Rietveld refinement showed that the two compounds crystallise in the cubic symmetry with Pm–3m space group, which is consistent with the value of the Goldschmidt tolerance factor t_G:

$$t_G = \frac{\langle r_A \rangle + r_O}{\sqrt{2}(\langle r_B \rangle + r_O)} \quad (1)$$

(see Table 1). Here $\langle r_A \rangle$, $\langle r_B \rangle$ and r_O are respectively the average ionic radii of the A and B perovskite sites and oxygen anion. The obtained structure refinement parameters are given in Table 1. We can see in this table that the cell volume increases slightly with the titanium doping. This is the first indication of the incorporation of titanium in the manganese site suggesting that titanium is in a tetravalent state [9,10] substituting the Mn^{4+} ion with a lower ionic radius ($r_{Mn4+} = 0.53$ Å $< r_{Ti4+} = 0.605$ Å for 6-fold coordination [11]). The increase of the cubic cell parameter is in good agreement with the results obtained by Zhong et al. [8] for oxygen deficient compounds $La_{2/3}Ba_{1/3}MnO_{3-\delta}$.

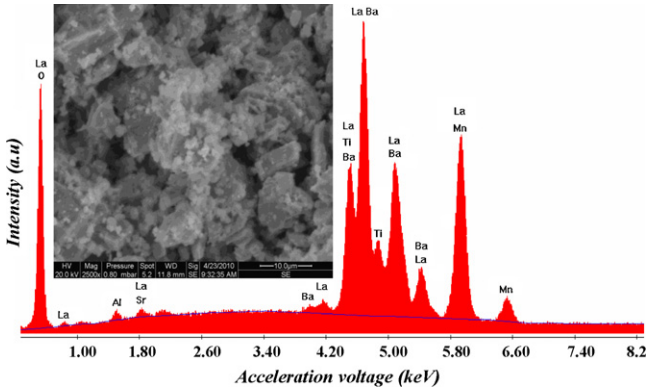

Fig. 2. Plot of EDX analysis of chemical species of sample $La_{0.67}Ba_{0.33}Mn_{0.98}Ti_{0.02}O_3$ giving a close composition to the nominal one as indicated in Table 1. The inset represents the SEM micrograph of the sample.

EDX plot of $La_{0.67}Ba_{0.33}Mn_{0.98}Ti_{0.02}O_3$ compound is shown in Fig. 2 and the resulted cations proportions are indicated in Table 1. Results of the quantitative ICPAES analysis of chemical species, especially for the oxygen content, are very close to the nominal ones within the experimental uncertainties (see Table 2) and, since no secondary phases are seen in the XRD patterns, it is reasonable to assume that Ti has been substituted for Mn in this sample. SEM micrograph of the sample is shown in the inset of Fig. 2. Morphology analysis of the micrograph revealed that the particles of the sample show some tendency towards agglomeration and the average particle size is ~2 μm. The average crystallites size was also calculated using the XRD data applying the Rietveld refinement formula

$$G_S = \frac{180\lambda}{\pi\sqrt{IG}} \quad (2)$$

where λ is the X-ray wavelength and IG is the Gaussian size parameter given by Rietveld refinement. As it can be seen in Table 1, the average grain size (G_S) estimated by X-ray analysis is ~30 nm for the two samples suggesting that very low Ti-doping level should not induce size effects on magnetic and magnetocaloric properties of these materials. This is not the case in the work of Tang et al. [12], which shows an increase of the grain size when the annealing temperature of $La_{0.7}Ca_{0.2}Ba_{0.1}MnO_3$ increases, which induced a significant change in magnetic and magnetocaloric properties.

3.2. Magnetization investigation

Fig. 3 displays the temperature dependence of the ZFC and FC magnetizations $M(T)$ for $La^{3+}{}_{2/3}Ba^{2+}{}_{1/3}Mn^{3+}{}_{2/3}Mn^{4+}{}_{1/3-0.02}Ti^{4+}{}_{0.02}O_3$ ($La_{0.67}Ba_{0.33}Mn_{0.98}Ti_{0.02}O_3$) sample. We can see in this figure that the low field (0.01 T) ZFC and FC magnetizations sharply increase near T_C (~314 K) determined from a linear extrapolation of $M(T)$ to zero magnetization (Fig. 3, main panel), or T_C (~309 K) determined from the dM/dT curve (a-inset of Fig. 3). A very close value was found by Zhong et al. [8] for the oxygen deficient compound $La^{3+}{}_{2/3}Ba^{2+}{}_{1/3}Mn^{3+}{}_{2/3}Mn^{4+}{}_{1/3-0.01}O^{2-}{}_{2.98}$ ($T_C = 312$ K) which presents a quite similar Mn^{4+}/Mn^{3+} (0.48) ratio to the one found in this work (0.47). The undoped compound $La_{0.67}Ba_{0.33}MnO_3$ has a relatively high Curie temperature, $T_C = 350$ K, as reported by Osthöver et al. in Ref. [7]. Interestingly an extremely low doping by non-magnetic Ti^{4+} replacing Mn^{4+}, reduces T_C by about 40 K, making it to be very close to room temperature, which is suitable for magnetic refrigeration. The decrease of T_C can be ascribed to the replacement of some of Mn^{3+}–O^{2-}–Mn^{4+} bonds by Mn^{3+}–O^{2-}–Ti^{4+} bonds which hampers the electron transfer through the Mn^{3+}–O^{2-}–Mn^{4+} network. Thus the decrease of T_C

Table 1
Columns 1, 2 and 3 represent the room temperature structural parameters (Rietveld refinement) for single phase cubic Pm–3m $La_{0.67}Ba_{0.33}Mn_{1-x}Ti_xO_3$ ($x = 0, 0.02$) compounds. The numbers in parentheses are estimated standard deviations to the last significant digit. Column 4 represents EDX analysis of the chemical species proportion.

	$La_{0.67}Ba_{0.33}Mn_{1-x}Ti_xO_3$ Phase cubic Pm–3m		EDX analysis % and proportion of cations for $x = 0.02$ compound
x	0	0.02	%La 36.85 → 0.681La
a (Å)	3.9075 (2)	3.9119 (2)	%Ba 17.23 → 0.319Ba
V (Å^3)	59.66 (0)	59.86 (1)	%Mn 44.83 → 0.977Mn
Density(g cm^{-3})	6.719	6.693	%Ti 1.06 → 0.023Ti
Goldschmidt factor t_G	0.9999	0.9992	
La/Ba B_{iso} (Å^2)	0.32 (9)	0.08 (4)	
Mn/Ti B_{iso} (Å^2)	0.02	0.066	
(O) B_{iso} (Å^2)	2.03 (9)	1.20 (1)	
$d_{(Mn,\,Ti)-O}$ (Å)	1.953 (5)	1.956 (2)	
$\theta_{(Mn,\,Ti-O-Mn,\,Ti)}$ (°)	180 (8)	180 (2)	
Band width W (a.u.)[a]	0.0961	0.0955	
Grain size G_S (nm)	29.00	31.51	
R_{wp} (%)	3.38	5.03	
R_p (%)	2.18	3.73	
R_F (%)	1.94	3.16	
χ^2 (%)	5.3	3.63	

[a] W (a.u) $\propto \frac{\cos[(1/2)(\pi-\theta_{Mn-O-Mn})]}{(d_{Mn-O})^{3.5}}$ [13].

Table 2
Atomic composition of chemical species for $La_{0.67}Ba_{0.33}Mn_{1-x}Ti_xO_3$ ($x = 0$, 0.02) samples as deduced from ICPAES analyses. The numbers in parentheses are estimated uncertainties to the last significant digit. Last column summarizes the as determined manganite formula which is very close to the nominal one if we consider such uncertainties.

	Chemical species					Manganite formula
x	La	Ba	Mn	Ti	O	
0	0.65(1)	0.32(1)	1.00(2)	–	2.95(8)	$La_{0.65}Ba_{0.32}MnO_3$
0.02	0.65(1)	0.31(1)	0.97(2)	0.025(6)	2.96(7)	$La_{0.65}Ba_{0.31}Mn_{0.97}Ti_{0.03}O_3$

is related to the decrease in the bandwidth W [13] (see Table 1) reducing the double exchange (DE) interactions [14]. Below T_C, the sample shows low field magnetization behaviour of a typical ferromagnet (FM). At higher temperature, above T_C (b-inset of Fig. 3) $M(T)$ follows a Curie–Weiss (CW) behaviour [15]. Between 340 and 400 K the material is still in the paramagnetic (PM) phase but due to short range order, a significant deviation from the high-T mean field behaviour is observed below 340 K (see the b-inset of Fig. 3 showing a small bump in the $1/\chi$ vs. T curve) leading to a larger experimental paramagnetic effective moment

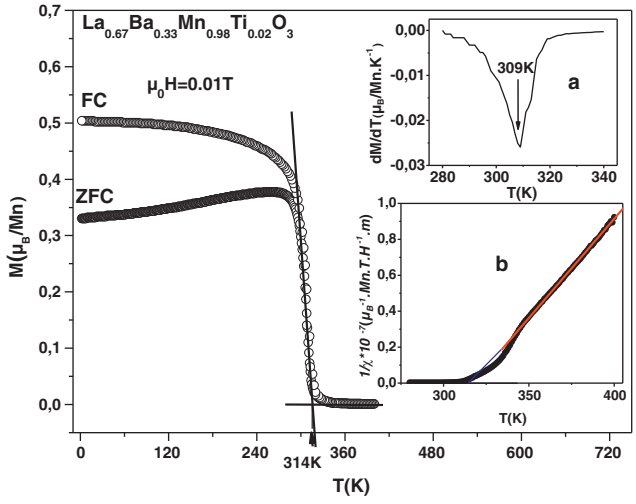

Fig. 3. (For interpretation of the references to colour in this figure legend, the reader is referred to the web version of the article.). $M(T)$ curves for $La_{0.67}Ba_{0.33}Mn_{0.98}Ti_{0.02}O_3$ sample at $\mu_0 H = 0.01$ T magnetic field in FC and ZFC modes. The a-inset is the dM/dT curve. The b-inset shows the inverse of the magnetic susceptibility ($1/\chi$) vs. T curve (The red line represents the linear fit of data and the blue line is our extrapolation to the temperature axis of this linear fit).

($\mu_{eff} = 5.69\,\mu_B$) than the value theoretically predicted ($4.48\,\mu_B$) [15] using the Mn^{3+} and Mn^{4+} concentrations. This may be due to short range ferromagnetic clusters occurring in the bump's temperature range situated between CW temperature ($\Theta = 315$ K) and 340 K, and to the formation of magnetic polarons as was reported in Ref. [16].

3.3. Magnetic entropy change determination

Independently of the method used for T_C determination, we can suggest that the Curie temperature is slightly shifted from 310 K. That conclusion allows us to choose the temperature range for isothermal $M(H)$ measurements in which T_C is in the middle. This range was chosen between 230 and 390 K with a step of 10 K.

The main panel of Fig. 4 shows the isothermal magnetization curves for the sample $La_{0.67}Ba_{0.33}Mn_{0.98}Ti_{0.02}O_3$. Based on the thermodynamic theory, the magnetic entropy change (ΔS_M), which results from the spin ordering and which is induced by the variation of the applied magnetic field from 0 to H_{max}, depends on the temperature gradient of the magnetization and attains a maximum value around the Curie temperature, at which the magnetization decays most rapidly. The temperature dependence of the magnetic entropy change (ΔS_M) for $La_{0.67}Ba_{0.33}Mn_{0.98}Ti_{0.02}O_3$ sample at various magnetic fields ($0 \to 1$ T, $0 \to 2$ T, $0 \to 3$ T, $0 \to 4$ T and $0 \to 5$ T) are computed from Eq. (3) [2,17].

$$-\Delta S_M\left(\frac{T_1+T_2}{2}\right) = \frac{1}{T_2-T_1}\left[\int_0^H M(T_2,H)\,dH' - \int_0^H M(T_1,H)\,dH'\right] \quad (3)$$

using the isothermal $M(H)$ data as shown in the a-inset of Fig. 4. The maximum value of ΔS_M, i.e. $|\Delta S_M^{max}|$ at each field is obtained near T_C. An attempt to the theoretical modeling of the magnetocaloric effect (MCE) was done by Amaral et al. [17] based on Landau theory

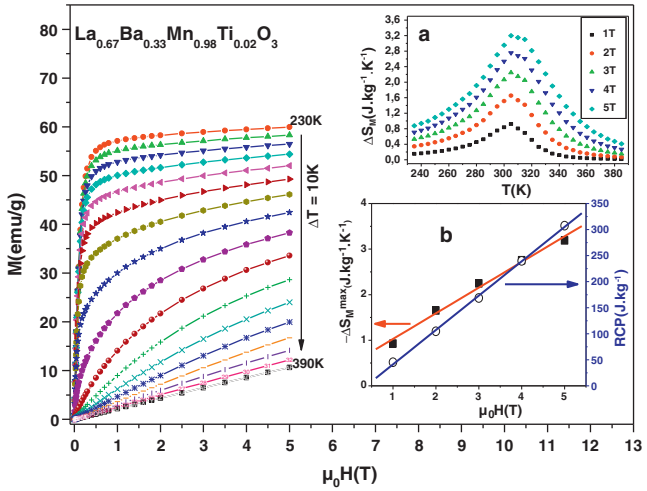

Fig. 4. Magnetization vs. applied magnetic field $\mu_0 H$, measured at different temperatures, for the $La_{0.67}Ba_{0.33}Mn_{0.98}Ti_{0.02}O_3$ sample. Data were taken at temperature steps of 10 K. The a-inset represents the temperature dependence of the magnetic entropy change (ΔS_M) under different applied magnetic fields. The b-inset represents the maximum entropy change $|\Delta S_M^{max}|$ and the relative cooling power (*RCP*) values vs. applied magnetic field.

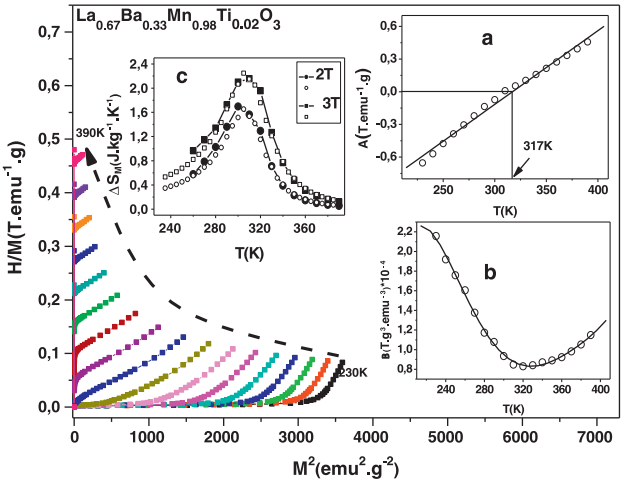

Fig. 5. Arrott plots H/M vs. M^2 using Eq. (5) at different temperatures showing a second order transition (positive slope) for $La_{0.67}Ba_{0.33}Mn_{0.98}Ti_{0.02}O_3$. The a-inset represents the parameter A vs. T. The b-inset shows the parameter B vs. T. The c-inset represents a comparison between experimental (open symbols) and theoretical predictions (full symbols) using the Landau theory, Eq. (6), for the entropy change ΔS_M under applied fields of 2 and 3 T.

of phase transition. At the Curie point of ferromagnets, it has been suggested that the magnetic energy MH needs to be included in the expression for the Gibbs free energy:

$$G(T, M) \cong G_0 + \frac{1}{2}A(T)M^2 + \frac{1}{4}B(T)M^4 - MH \quad (4)$$

where the coefficients A and B are temperature-dependent parameters containing the elastic and magnetoelastic terms of free energy [18]. From the equilibrium condition $\partial G/\partial M = 0$, a magnetic equation of state can be derived

$$\frac{H}{M} \cong A(T) + B(T)M^2 \quad (5)$$

The Arrott plots H/M vs. M^2 extracted from the experimental isothermal $M(T, H)$ curves are shown in Fig. 5. These plots give a positive slop in the complete M^2 range which confirms that our sample exhibits a second order FM–PM phase transition, according to the Banerjee criterion [19]. The magnetic entropy change obtained from Gibbs' free energy using Eq. (4) is

$$S(T, M) \cong -\frac{1}{2}A'(T)M^2 - \frac{1}{4}B'(T)M^4 \quad (6)$$

where $A'(T)$ and $B'(T)$ are the temperature derivatives of the expansion coefficients. The temperature dependence of the parameters A and B is obtained from the linear region of the Arrott plot of Eq. (5). Thermal variation of the parameter A is found to be almost linear (a-inset of Fig. 5), whereas the temperature dependence of parameter B is highly nonlinear (b-inset of Fig. 5). The nature of the parameter B takes a crucial role in determining ΔS_M as suggested by Amaral et al. [17]. Using the thermal variation of the A and B parameters (a- and b-insets of Fig. 5), the temperature dependence of ΔS_M is calculated from Eq. (6), under magnetic fields of 2 and 3 T. The c-inset of Fig. 5 shows a good agreement between the Landau plot (full symbols) and the experimental plot (open symbols) of ΔS_M vs. T for the $La_{0.67}Ba_{0.33}Mn_{0.98}Ti_{0.02}O_3$ sample, suggesting that the magnetoelastic coupling and the electron interaction influence [17,18] are important factors in the study of the magnetocaloric properties of this material.

The magnetic cooling efficiency of a magnetocaloric material is evaluated by considering the relative cooling power (*RCP*) [20,21]. For a magnetic refrigerator, the engineer or designer needs to know the cooling per unit volume, and thus the only units which are meaningful for such comparisons are mJ cm^{-3} K^{-1}, and for this reason we have converted the ΔS_M and *RCP* values of our material into volumetric entropy units, since the J kg^{-1} K^{-1} units are easily converted to the mJ cm^{-3} K^{-1} values if the density of material is known, which is the case in this work (see Table 1). The magnetic entropy change ΔS_M near T_C is arising from the interactions between the Mn spin systems. $|\Delta S_M^{max}|$ and *RCP* exhibit an almost linear rise with increasing field, as shown in the b-inset of Fig. 4, which is an indication of much larger entropy change and relative cooling power to be expected at higher magnetic field ($|\Delta S_M^{max}| = 3.21$ J kg^{-1} K^{-1} or 21.48 mJ cm^{-3} K^{-1} and *RCP* = 307 J kg^{-1} or 2054 mJ cm^{-3} at 5 T), signifying therefore the effect of spin–lattice coupling associated to changes in the magnetic ordering process in the sample.

In Table 3 we compare our performances of MCE with some others reported in the literature. On one hand we note that our $|\Delta S_M^{max}|$, 0.93 J kg^{-1} K^{-1} (6.22 mJ cm^{-3} K^{-1}) for 1 T, is about 30% of that of pure Gd [2], but our ΔS_M distribution is much more uniform

Table 3
Maximum entropy change, $|\Delta S_M^{max}|$ and relative cooling power (*RCP*) occurring at the Curie temperature (T_C) and at a magnetic field, $H = 1$ or 5 T, for $La_{0.67}Ba_{0.33}Mn_{0.98}Ti_{0.02}O_3$ compared to several materials considered for magnetic refrigeration.

Composition	T_C (K)	ΔH (T)	$-\Delta S_M$ (J kg^{-1} K^{-1})	*RCP* (J kg^{-1})	Ref.
Gd	293	1	3.25	–	[2]
Gd	293	5	9.5	410	[20–24]
$Gd_5Si_2Ge_2$	275	5	18.5	535	[20–24]
$La_{2/3}Ba_{1/3}MnO_3$	337	1	2.70	68	[8]
$La_{0.67}Ba_{0.33}Mn_{0.98}Ti_{0.02}O_3$	314	1	0.93	45	This work
$La_{2/3}$ $Ba_{1/3}MnO_{2.98}$	312	1	2.60	65	[8]
$La_{0.67}Ba_{0.33}MnO_3$	292	5	1.48	161	[22]
$La_{0.67}$ $Ba_{0.33}Mn_{0.98}Ti_{0.02}O_3$	314	5	3.24	307	This work

(see the a-inset of Fig. 4) than that of pure Gd, which is desirable for an Ericsson-cycle magnetic refrigerator [1]. On the other hand, our $|\Delta S_M^{max}|$ is larger than that of $La_{0.67}Ba_{0.33}MnO_3$ [22], somewhat smaller than the one of the oxygen deficient $La_{2/3}Ba_{1/3}MnO_{3-\delta}$ [8], and much smaller than those of the pseudo binary alloy $Gd_5Si_2Ge_2$ [23,24] and $MnFeP_{1-x}As_x$ and $Mn_{1.2}FeP_{1-x}Ge_x$ pnictides [25]. However we note that our $La_{0.67}Ba_{0.33}Mn_{0.98}Ti_{0.02}O_3$ specimen exhibits a large relative cooling power *RCP* and can thus be used as an active magnetic refrigerator in a relatively wide range of temperatures near 310 K, with a relatively large entropy change.

4. Conclusion

Synthesis and structural characterization of $La_{0.67}Ba_{0.33}Mn_{0.98}Ti_{0.02}O_3$ manganite were performed. X-ray analyses reveal that this material is isostructural to $La_{2/3}Ba_{1/3}MnO_{3-\delta}$ reported by Zhong et al. and crystallising in cubic Pm–3m structure. Measurements of magnetization showed a sharp paramagnetic–ferromagnetic transition with Curie temperature (T_C) nearing the room temperature and very close to that reported by Zhong et al. for $La_{2/3}Ba_{1/3}MnO_{3-\delta}$. Above T_C, between 340 and 400 K, the material follows well Curie–Weiss law. But due to short range order, a significant deviation from the high-T mean field behaviour is observed below 340 K leading to significantly larger effective paramagnetic moment than the one theoretically predicted. This significant difference should be ascribed to the formation of local ferromagnetic clusters and magnetic polarons. Magnetocaloric behaviour of this specimen was examined from isothermal magnetization vs. magnetic field data measured at different temperatures surrounding Curie temperature T_C. We found that experimental magnetic entropy matched well with the theoretical one determined using the Landau theory. The maximum value of the magnetic entropy change obtained from the $M(H)$ plot data is $|\Delta S_M^{max}| = 21.48\,mJ\,cm^{-3}\,K^{-1}$ and the relative cooling power (*RCP*) is $2054\,mJ\,cm^{-3}$ under an applied magnetic field of 5 T, and $La_{0.67}Ba_{0.33}Mn_{0.98}Ti_{0.02}O_3$ can thus be used as an active magnetic refrigerator in a relatively wide range of temperatures nearing 310 K, with a relatively large entropy change.

Acknowledgements

Authors acknowledge the Tunisia–France exchange program DGRS–CNRS project no. 09//R 11-52

References

[1] G.V. Brown, J. Appl. Phys. 47 (1976) 3673.
[2] M. Földeàki, R. Chachine, T.K. Bose, J. Appl. Phys. 77 (7) (1995) 3528.
[3] R. von Helmolt, J. Wecker, B. Holzapfel, L. Schultz, K. Samwer, Phys. Rev. Lett. 71 (1993) 2331.
[4] S. Gupta, R. Ranjit, C. Mitra, P. Raychaudhuri, R. Pinto, Appl. Phys. Lett. 78 (2001) 362.
[5] V.S. Kolat, H. Gencer, S. Atalay, Physica B 371 (2006) 199.
[6] Anis Biswas, Tapas Samanta, S. Banerjee, I. Das, Appl. Phys. Lett. 92 (2008) 212502.
[7] C. Osthöver, P. Grünberg, R.R. Arnos, J. Magn. Magn. Mater. 177 (1998) 854–855.
[8] W. Zhong, W. Chen, C.T. Au, Y.W. Du, J. Magn. Magn. Mater. 261 (2003) 238.
[9] A. Gasmi, M. Boudard, S. Zemni, F. Hippert, M. Oumezzine, J. Phys. D: Appl. Phys. 42 (2009) 225408.
[10] A.N. Ulyanov, Y.M. Kang, S.I. Yoo, D.S. Yang, H.M. Park, K.W. Lee, S.C. Yu, J. M. M. M. 304 (2006) 331–333.
[11] R.D. Shannon, Acta Crystallogr. A 32 (1976) 751–764.
[12] W. Tang, W.J. Lu, X. Luo, B.S. Wang, X.B. Zhu, W.H. Song, Z.R. Yang, Y.P. Sun, Physica B 405 (2010) 2733–2741.
[13] P.-G. Radaelli, G. Iannone, M. Marezio, H.-Y. Hwang, S.-W. Cheong, J.-D. Jorgensen, D.-N. Argyriou, Phys. Rev. B 56 (1997) 8265.
[14] C. Zener, Phys. Rev. B 82 (1951) 403.
[15] C. Kittel, Introduction to Solid State Physics, Wiley, New York, sixth ed., pp. 404–406.
[16] B. Martinez, V. Laukhin, J. Fontcuberta, L. Pinsard, A. Revcolevschi, Phys. Rev. B 66 (2002) 054436.
[17] J.S. Amaral, V.S. Amaral, J. Magn. Magn. Mater. 322 (2010) 1552.
[18] L.P. Lévy, Magnetism and Superconductivity, Springer, Berlin, 2000.
[19] B.K. Banerjee, Phys. Lett. 12 (1964) 16.
[20] V.K. Pecharsky, K.A. Gschneidner, A.O. Tsokol, Rep. Prog. Phys. 68 (2005) 1479.
[21] M.H. Phan, S.C. Yu, J. Magn. Magn. Mater. 308 (2007) 325.
[22] D.T. Morelli, A.M. Mance, J.V. Mantese, A.L. Micheli, J. Appl. Phys. 79 (1996) 373.
[23] V.K. Pecharsky Jr., K.A. Gschneidner, Phys. Rev. Lett. 78 (23) (1997) 4494.
[24] V.K. Pecharsky Jr., K.A. Gschneidner, J. Magn. Magn. Mater. 167 (1997) L179.
[25] Z.Q. Ou, G.F. Wang, S. Lin, O. Tegus, E. Brück, K.H.J. Buschow, J. Phys.: Condens. Matter 18 (2006) 11577–11584.